Topological Interface between Pfaffian and Anti-Pfaffian Order in $\nu = 5/2$ Quantum Hall Effect

W. Zhu,[1] D. N. Sheng,[2] and Kun Yang[3]

[1]*Institute of Natural Sciences, Westlake Institute of Advanced Study, Hangzhou, 030024, China*
and School of Science, Westlake University, Hangzhou, 030024, China
[2]*Department of Physics and Astronomy, California State University, Northridge, California 91330, USA*
[3]*National High Magnetic Field Laboratory and Physics Department, Florida State University, Tallahassee, Florida 32306, USA*

A recent thermal Hall experiment triggered renewed interest in the problem of $\nu = 5/2$ quantum Hall effect, which motivated novel interpretations based on the formation of mesoscopic puddles made of Pfaffian and anti-Pfaffian topological orders. Here, we study an interface between the Pfaffian and anti-Pfaffian states, which may play crucial roles in thermal transport, by means of state-of-the-art, density-matrix renormalization group simulations. We demonstrate that an intrinsic electric dipole moment emerges at the interface, similar to the "*p-n*" junction sandwiched between *N*-type and *P*-type semiconductor. Importantly, we elucidate the topological origin of this dipole moment, whose formation is to counterbalance the mismatch of guiding-center Hall viscosity of bulk Pfaffian and anti-Pfaffian states. In addition, these results imply that the formation of a dipole moment could be helpful to stabilize the puddles made of Pfaffian and anti-Pfaffian states in experimental conditions.

The $\nu = 5/2$ fractional quantum Hall (FQH) effect in the second Landau level has sparked much interest in condensed matter for decades [1–12], mainly due to its likely non-Abelian nature and potential application in topological quantum computation [13,14]. The leading theoretical candidate is the non-Abelian Pfaffian (PF) state [15,16], a fully polarized chiral *p*-wave state of composite fermions [17], as supported by numerical studies [18–30]. Besides, its particle-hole conjugate partner, known as the anti-Pfaffian (APF) state [31,32], is an equally valid candidate, which may actually be more viable under realistic experimental conditions [33–36]. Breaking of particle-hole symmetry, either spontaneously or explicitly, is crucial for the emergence of the PF or APF state. Recently, to interpret the observation of half-integer thermal Hall conductance that is consistent with particle-hole symmetry [37], the particle-hole preserved PF state was proposed [38,39]. Alternatively, the experimental observation could be simply explained by lack of thermal equilibration at the edge [40] (a scenario currently under debate [41–43]), or, more significantly, by the presence of random domains made of the PF and APF states [44–46], similar to an earlier proposal of spontaneously formed PF and APF strips [47]. The latter makes understanding of PF-APF domain walls an urgent priority.

Generally speaking, the topologically protected edge states directly reflect bulk topological order via the bulk-edge correspondence [48–51], rendering edge the preferred window to peek into the fascinating bulk physics in topological states of matter [52–55]. In the particular case of non-Abelian PF-type states, this correspondence leads to the presence of neutral Majorana fermion modes at the edge [56] (i.e., the interface separating the bulk from vacuum) responsible for the half-integer quantized thermal Hall conductance [37]. Relatively speaking, less attention is drawn to the interface between two distinct topological states [46,57–71], especially for those separating two non-Abelian orders [47,72–74]. Existing theoretical attempts mostly rely on the effective field theories, where novel phenomena may emerge through the coupling between the two edges that meet at the interface. While such phenomenological theory is good at obtaining a qualitative understanding of the possible phases, many open questions remain and call for quantitative study by unbiased numerical approaches [68,69]. For example, it is extremely difficult for effective theories to determine which interface state is energetically favored by the microscopic interactions, as well as nonuniversal aspects like edge reconstruction [75–78], which, in principle, could also happen at the interface [66]. Numerical simulation is expected, in a quantitative and unbiased way, to overcome these challenges faced by effective field theories. It is therefore highly desirable and urgent to develop an advanced numerical scheme to address some pressing problems like the PF-APF interface.

In this Letter, we construct an interface between the PF and APF state, based on which, we investigate the underlying physics of PF-APF domain wall in the FQH effect at the filling factor $\nu = 5/2$. Our approach is based on a design of cylinder geometry by utilizing the density-matrix

renormalization group (DMRG) algorithm. We establish that the edge modes of the PF and APF states strongly hybridize near the interface, indicating that counter-propagating charge modes are fully gapped out. We show the appearance of charge inhomogeneity around the interface, which yields a robust electric dipole moment. Crucially, we identify the mismatch of Hall viscosity between the PF and APF topological orders as the driving force behind this dipole moment, thus revealing the topological content of the PF-APF interface, whose possible experimental consequences will be also discussed.

Model and method.—We consider interacting electrons in the presence of a perpendicular magnetic field on the cylinder geometry. In the Landau gauge $\mathbf{A} = (0, Bx)$, the single-particle orbital in Nth Landau level is $\psi_m(x, y) = (1/\sqrt{2^N N! L_y \ell \sqrt{\pi}}) e^{ik_m y} e^{-[(x-k_m \ell^2)^2/2\ell^2]} H_N(x - k_m \ell^2/\ell)$, where the momentum along the circumference is $k_m = (2\pi m/L_y)$, and m labels the orbital center position $x_m = k_m \ell^2$ along the cylinder axis ($\ell = \sqrt{\hbar/eB}$ is the magnetic length). When the magnetic field is strong, by projecting onto the second Landau level, the many-body Hamiltonian is written as (see Ref. [79])

$$\hat{H} = \sum_{\{m_i\}} V_{m_1, m_2, m_3, m_4} \hat{a}_{m_1}^\dagger \hat{a}_{m_2}^\dagger \hat{a}_{m_3} \hat{a}_{m_4}, \qquad (1)$$

where $a_m^\dagger (a_m)$ is the creation (annihilation) operator of an electron in the orbital m, and V represents matrix elements of modified Coulomb interaction $(1/r)e^{-(r^2/\xi^2)}$, with a regulated length $\xi = 4\ell$ [33,79]. Throughout the Letter, total filling fraction is set to be half filled in the second Landau level.

For numerical calculations, we apply a suitable DMRG algorithm with multiple steps for such an interface system. The DMRG algorithm is based on the matrix product state representation of the ground state: $|\Psi A_m^{[n_m]}\rangle) = \dots A_0^{[n_0]} A_1^{[n_1]} \dots |\dots, n_0, n_1, \dots\rangle$, where $A_m^{[n_m]}$ are $D \times D$ matrices, and $\{n_m\} = 0, 1$ represents the occupancy on orbital m. In order to model the interface, we perform the "cut-and-glue" scheme, by combining finite DMRG [86] and infinite DMRG [87] algorithms, as discussed below. First, the infinite DMRG is used to iteratively minimize ground state energy $E_0 = \langle \Psi(A_m^{[n_m]}) | \hat{H} | \Psi(A_m^{[n_m]}) \rangle$ by optimizing $A_m^{[n_m]}$ on an infinite cylinder [80], which allows us to obtain the optimized PF or APF state separately. This procedure has proven to be efficient in the study of FQH ground states ranging from Abelian to non-Abelian systems [33,80,84]. Second, based on the optimized PF (APF) state living on the infinite cylinder, we cut both of them into two halves and then glue $A_m^{[n_m]}$ ($m < 0$) from the PF state (shaded in blue) together with $A_m^{[n_m]}$ ($m \geq 0$) from the APF state (shaded in red), which yields an interface between the
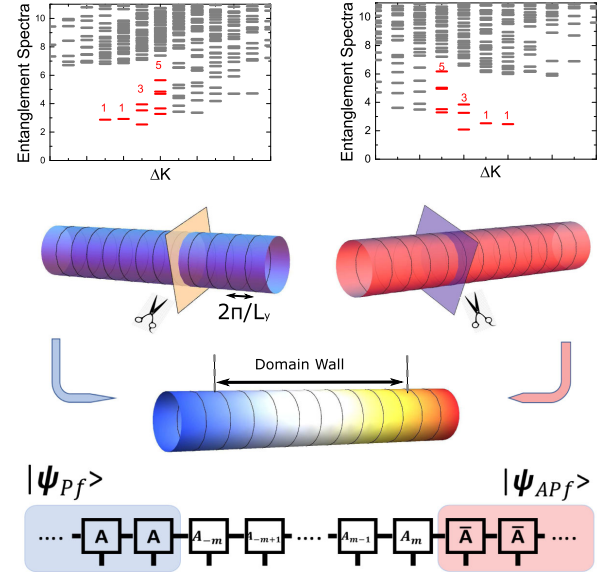
FIG. 1. Interface between the PF and APF topological order on the cylinder geometry. Top: Typical orbital entanglement spectra for gapped PF (left) and APF (right) state. The chiral dispersions revealed in the entanglement spectra reflect spontaneous breaking of particle-hole symmetry. Middle: Schematic representation of the PF-APF interface in the Landau orbital (labeled as black circle) space on the cylinder geometry. We first cut the PF (APF) state into two halves and glue the left part of the PF state and right part of the APF state together, which creates an interface regime sandwiched between the PF and APF states. Bottom: The MPS representation of the PF-APF interface.

PF and APF states (as graphically shown in Fig. 1). This "glue" scheme has been verified with model wave functions [68,69]. Third, by fixing the end of the PF (APF) state as the left (right) boundary, we optimize the state via finite DMRG on a finite segment enclosing L_M orbitals (up to $L_M = 320$) embedded in the middle of the infinite cylinder.

Here, we would like to point out methodological advantages of our scheme. First, on the infinite cylinder, the PF and APF states are automatically selected resulting from spontaneous particle-hole symmetry breaking and are treated on equal footing without any bias. Second, one can use established techniques, e.g., entanglement spectra via a cylinder bipartition [29,33,49], as a probe of the PF (APF) topological order (see Fig. 1, top). Third, the microscopic state of the interface can be resolved accurately. Our calculation is based on a microscopic Hamiltonian instead of model wave functions [69], so the domain wall structure shown below represents the energetically favorable state at the interface.

Interface structure.—We start by discussing the effective edge theories of the PF and APF states [31,51,56,88] (for details see Ref. [79]). There are two possible edge structures across the interface, depending on the strength of coupling between them [74]. If the tunneling effect across the interface is irrelevant, the edge modes of the PF and
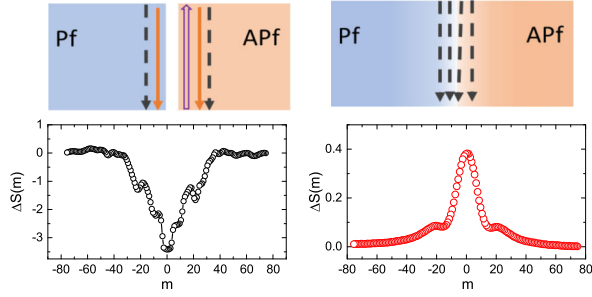
FIG. 2. Interface structures distinguished by entanglement entropy. The interface structure in the weak coupling limit (top left) and in the strong hybridization case (top right). Here, black dashed lines represent the neutral chiral Majorana fermion modes, and solid lines represent chiral boson modes of different kinds (for details, see [79]). Bottom: The calculated entanglement entropy $\Delta S(m) = S(m) - S_{\mathrm{PF(APF)}}$ dependence on bipartition position m. ($m = 0$ is the center of the interface.) The entanglement entropy develops a dip in the weak coupling limit (bottom left) and a peak structure in the strong hybridization case (bottom right). The cylinder perimeter is set to be $L_y = 19\ell$, and the bond dimension is $D = 3600$.

APF states form two (nearly) independent sets, sitting on the left and right side of the interface (see Fig. 2, top left). In this case, if an entanglement measurement is performed, we expect a minimum of the entanglement entropy at the interface, reflecting the effectively decoupled nature between the PF and APF states. On the other hand, if the tunneling process across the interface is strong, the counterpropagating charge modes gap out due to the hybridization effect. As a result, the PF-APF interface hosts four copropagating neutral majorana modes [44–47] (see Fig. 2, top right), allowing neutral fermion to directly tunnel across the interface. Thus, we expect to see massive entanglement around the interface as a signal of gapless modes.

Motivated by this intuition, we compute the entanglement entropy and its dependence on the entanglement cut position. We first create uncoupled edges by turning off interaction terms crossing the interface. In this case, we observe a dip in entanglement at the interface (Fig. 2, bottom left). As a comparison, the result with full (translationally invariant) interaction is shown in Fig. 2, bottom right. Far away from the interface, the entanglement entropy converges to the value of the PF (APF) state. Near the interface, the entanglement entropy develops a peak centered at the interface. The appearance of enhanced entanglement across the interface favors the strong coupling picture (Fig. 2, top right) and suggests that charged modes are fully gapped out and only neutral modes survive around the PF-APF interface (see [79]).

Intrinsic interface dipole moment and Hall viscosity.—In spite of the absence of charged modes, we identify emergent charge fluctuation around the interface. Figure 3 shows the charge distribution along the cylinder
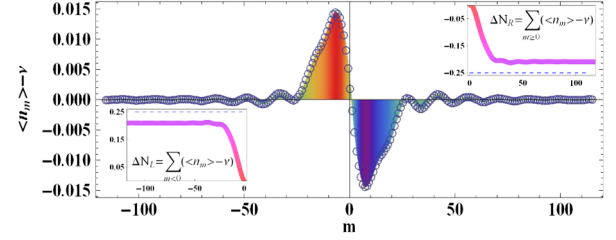
FIG. 3. Domain wall structure at the interface. The charge distribution profile $\langle n_m \rangle - \nu$ (open circles) along the cylinder, where the leftmost (rightmost) side is a uniform PF (APF) state. The colored shade denotes the deviation from uniform distribution $\nu = 1/2$. The integration of the difference between the actual occupation number and the uniform occupation number on the left half ΔN_L (bottom left inset) and on the right half ΔN_R (bottom right inset). The cylinder perimeter is set to be $L_y = 19\ell$, and the bond dimension is $D = 3600$.

axis. One salient feature is that charge profile smoothly interpolates between the PF and the APF state, and a profound charge fluctuation appears around the interface with small ripples in the periphery of the interface. In particular, we identify that the PF (APF) side contains an excess of electron (holelike) chargers. [The electron (hole)-rich region switches, if we swap the position of PF (APF) state in Fig. 1.] For quantitative description, Fig. 3 (inset) depicts the accumulation of charge on the left and right side of the interface. We find several notable features. First, total charge on the left (right) part of the interface gives $\Delta N_L \approx -\Delta N_R$ (in unit of e), where we define the net charge accumulation as $\Delta N_{L(R)} = \sum_{m \lessgtr 0}[\langle n_m \rangle - \nu]$. Importantly, the total charge on each side of the interface is equal but takes the opposite sign, which results in a neutral charge condition without net charge accumulation. Second, due to the hybridization effect near the interface, the net charge on the left (right) side is not quantized, which is dependent on the details of the interface (e.g., cylinder circumference L_y) [79]. Third, we identify the domain wall region with a spatial length scale $d_{\mathrm{PF}} + d_{\mathrm{APF}}$, [the distance that domain wall penetrates into the PF (APF) side]. We estimate $d_{\mathrm{PF}} \approx d_{\mathrm{APF}} \sim 8\ell$, and it is slightly larger than previous estimation of quasihole radii based on the PF model wave function [89]. Last, we would like to point out that the above finding is similar to that of the "*p-n*" junction in the semiconductor, where the neutrality is lost near the *p-n* interface, and the mobile charge carriers form the depletion layer. Interestingly, different from the *p-n* junction, next, we will show the origin of charge inhomogeneity at the PF-APF interface is topological.

To gain some physical intuition of the appearance of electric charge inhomogeneity, we first try to consider empirical analysis in the thin-torus limit [90,91]. The typical root configuration pattern of the PF state is …01100110…, corresponding to a generalized Pauli principle of no more than two electrons in four consecutive

orbitals. The APF root configuration is simply its particle-hole conjugate. In order to switch from one pattern to the other, defects must be introduced near the interface, and the simplest one that does not change particle number is $\ldots 0110011_\times 0|1_\circ 0011001\ldots$, where the symbol $\times$ ($\circ$) denotes a quasielectron (quasihole) that emerges around the nearest four consecutive orbitals, and "|" labels the interface position. Therefore, quasielection-quasihole pairs naturally appear around the PF-APF interface, providing a direct understanding on the observation of domain wall in Fig. 3. Please note that the quasielectron and quasihole are close to each other, and hybridization effect should be strong, thus the charge of quasielectron (quasihole) is not well quantized. Moreover, although this empirical method is informative, it is not exact beyond the thin-torus limit. Next, we will elucidate the appearance of electric dipole around the interface is an intrinsic quantity of topological origin (see below).

The above discussion raises an interesting question: Is the formation of a dipole moment intrinsic to the PF-APF interface? Or, can the quasielectron and quasihole annihilate with each other accidentally? We now show that the dipole moment at the PF-APF interface indeed has topological origin by comparing the topological content of the two bulks. The PF (APF) state carries a different topological number, the guiding-center Hall viscosity [92–96] $\eta_H^{PF} = -\eta_H^{APF}$, where the Hall viscosity is determined by the guiding-center spin via $\eta_H = -(\hbar/4\pi\ell^2)(s/q)$ (in flat space-time metric). For the PF (APF) state, the orbital-averaged guiding center spin takes $(s^{PF}/q) = \frac{1}{2}$ and $(s^{APF}/q) = -\frac{1}{2}$ [81], respectively. Then, if the PF and APF states are put together, there should be a viscous force exerted on a segment of the interface with length dL_y: $dF^{visc} = (\eta_H^{PF} - \eta_H^{APF})B^{-1}\nabla_x E dL_y$ [B is the magnetic field, and $E(x, y)$ is the nonuniform electric field at the interface]. On the other hand, around the interface, the electric field coupled with the electric dipole leads to a force: $dF^{elec} = (\Delta p^x/L_y)\nabla_x E dL_y$. Here, we define the dipole moment density as $\Delta p^x/L_y = [p^x(-\infty) - p^x(\infty)]/L_y$, and $[p^x(k)/L_y] = -e\int_0^k p\ell^2[\langle n_p \rangle - \nu](dp/2\pi)$. If the interface is stable, we require the above two forces should be balanced $dF^{visc} + dF^{elec} = 0$. Therefore, we reach a relationship between the dipole moment density and Hall viscosity:

$$\frac{\Delta p^x}{L_y} = B^{-1}(\eta_H^{PF} - \eta_H^{APF}) = -\frac{e}{4\pi}\left(\frac{s^{PF}}{q} - \frac{s^{APF}}{q}\right). \quad (2)$$

In Fig. 4 (left), we show one typical dipole moment density dependence on momentum k across the interface. Since the PF (APF) state is uniform in its bulk, the dipole moment indeed converges to a finite value when k gets large enough. Crucially, the change of dipole moment density across the interface is $(\Delta p^x/L_y) \approx 0.99$ [in unit of
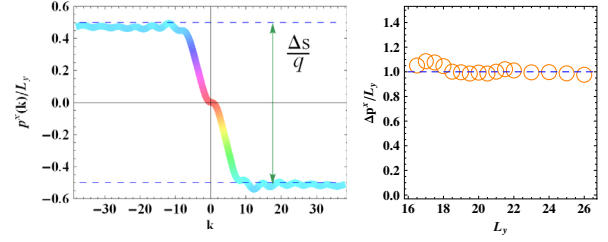
FIG. 4. Intrinsic dipole moment density near the interface. Left: Dipole moment density obtained by $p^x(k)/L_y = -e\int_0^k p\ell^2[\langle n_p \rangle - \nu](dp/2\pi)$ [in unit of $(-e/4\pi)$]. The blue dashed lines show predicted guiding-center spin $(s/q) = \frac{1}{2}(-\frac{1}{2})$ for the PF (APF) state. The system size is $L_y = 19\ell$. Right: The dipole moment density across the interface $\Delta p^x/L_y$ on various cylinder width L_y. The dashed line denotes the theoretical prediction $\Delta p^x/L_y = (s^{PF}/q) - (s^{APF}/q) = 1$.

$(-e/4\pi)$], close to the guiding-center spin difference $(s^{PF}/q) - (s^{APF}/q)$. In Fig. 4 (right), we demonstrate the numerically extracted dipole moment density for various cylinder width L_y, which is close to exact quantization for all system sizes that we can reach. As we can see, the dipole moment density is quantitatively in line with theoretical expectation. Thus, our results demonstrate that the formation of electric dipole is to counterbalance the difference of guiding-center Hall viscosity across the interface.

Generation of domain wall by disorder.—The above discussion demonstrates that the PF-APF domain wall hosts an intricate structure (Sec. D.3 [79]), which is overlooked in the effective edge theories [44–47]. It is worth noting that it makes the domain wall energetically favorable in the presence of an electric field. As a result, in a real sample, sufficiently strong disorder could potentially stabilize the PF-APF domain wall [97]. To be specific, we first estimate the domain wall tension around $\sigma \sim 2.2 \times 10^{-3}e^2/\ell^2$ (Sec. D.2 [79]). To balance it, the required electric field is around $E_{dis} \geq \sigma/(\Delta p^x/L_y) \sim 2.86 \times 10^5$ V/m (we set $\ell = 11.8$ nm for $B = 5$ T). It is largely in the same order with the typical disorder strength in the high-mobility GaAs/Ga$_{1-x}$Al$_x$As samples [79]. Based on this, we conclude the PF-APF domain wall could be stabilized in the current experimental condition.

Landau-leveling mixing effect.—Landau-level mixing breaks particle-hole symmetry and is important to the nature of the $\nu = 5/2$ state [24,33,34,82]. Here, we discuss the competition between the formation of PF-APF domain wall and Landau-level mixing effect (Sec. D4 [79]). We assume the puddles made of PF or APF liquids are formed in the system, and its typical size is L^{dw}. On one hand, due to the coupling between electric dipole and disorder potential, an energy gain is estimated to be $E_1^{dw} \approx -\sigma 4L^{dw}$ (here, we assume the dipole energy gain is of the same order as the domain wall tension based on our previous estimate). On the other hand, the Landau-level mixing effect induces an energy difference between PF and APF

states [33,82], $E_0 \approx 0.00066\kappa$ (per electron, in unit of e^2/ℓ, $\kappa \sim 1$ is the Landau-level mixing parameter [30]). Thus, the energy cost of each PF-APF puddle due to Landau-level mixing effect is estimated to be $E_2^{dw} \approx E_0 \nu[(L^{dw})^2/2\pi\ell^2]$. One can see that the above two energy scales have a different dependence on the domain wall size L^{dw}. Thus, there should exist a critical length $L_c^{dw} \sim (4\sigma/\nu E_0)2\pi\ell^2 \approx 167.51 \, \kappa^{-1}\ell$. When $L^{dw} < L_c^{dw}$, the energy scale due to the electric dipole moment predominates and the PF-APF domain wall could be stabilized, while the Landau-level mixing effect only becomes relevant if $L^{dw} > L_c^{dw}$. This mechanism should be robust against minor modification of assumptions (e.g., the estimated value σ, κ). In a word, even though the Landau-level mixing effect is considered, the formation of PF-APF domain wall could be energetically favorable in principle, under the condition of domain wall size below a critical value.

Summary and discussion.—We have presented compelling evidences that the interface between the Pfaffian (Pf) and anti-Pfaffian (APF) states has intrinsic topological properties. We identify an inhomogeneous charge distribution around the interface, where an excess of electron (hole) like chargers is pinned to the PF (APF) side, while the charge neutrality still holds on average. In particular, the characteristic charge profile yields an electric dipole at the interface, which is to counterbalance the mismatch in guiding-center Hall viscosity of the PF and APF state.

Our results unveil a notable effect on the PF-APF interface, which is overlooked in the previous discussions 47,82–44]]. This finding may shed lights on the stability of mesoscopic puddles made of PF and APF order [79]. In addition, the current Letter opens up a number of directions deserving further exploration. For example, it is an outstanding issue to characterize the topological nature of neutral chiral modes on the interface. Numerical studies may also further reveal rich physics of the interface made of other exotic non-Abelian states.

[1] R. Willett, J. P. Eisenstein, H. L. Störmer, D. C. Tsui, A. C. Gossard, and J. H. English, Phys. Rev. Lett. **59**, 1776 (1987).

[2] W. Pan, J.-S. Xia, V. Shvarts, D. E. Adams, H. L. Stormer, D. C. Tsui, L. N. Pfeiffer, K. W. Baldwin, and K. W. West, Phys. Rev. Lett. **83**, 3530 (1999).

[3] W. Pan, J. S. Xia, H. L. Stormer, D. C. Tsui, C. Vicente, E. D. Adams, N. S. Sullivan, L. N. Pfeiffer, K. W. Baldwin, and K. W. West, Phys. Rev. B **77**, 075307 (2008).

[4] H. C. Choi, W. Kang, S. D. Sarma, L. N. Pfeiffer, and K. W. West, Phys. Rev. B **77**, 081301(R) (2008).

[5] M. Dolev, M. Heiblum, V. Umansky, A. Stern, and D. Mahalu, Nature (London) **452**, 829 (2008).

[6] I. P. Radu, J. B. Miller, C. M. Marcus, M. A. Kastner, L. N. Pfeiffer, and K. W. West, Science **320**, 899 (2008).

[7] A. Bid, N. N. Ofek, H. Inoue, M. Heiblum, C. L. Kane, V. Umansky, and D. D. Mahalu, Nature (London) **466**, 585 (2010).

[8] R. L. Willett, C. Nayak, K. Shtengel, L. N. Pfeiffer, and K. W. West, Phys. Rev. Lett. **111**, 186401 (2013).

[9] M. Stern, P. Plochocka, V. Umansky, D. K. Maude, M. Potemski, and I. Bar-Joseph, Phys. Rev. Lett. **105**, 096801 (2010).

[10] L. Tiemann, G. Gamez, N. Kumada, and K. Muraki, Science **335**, 828 (2012).

[11] S. Baer, C. Rössler, T. Ihn, K. Ensslin, C. Reichl, and W. Wegscheider, Phys. Rev. B **90**, 075403 (2014).

[12] V. Venkatachalam, A. Yacoby, L. Pfeiffer, and K. West, Nature (London) **469**, 185 (2011).

[13] A. Kitaev, Ann. Phys. (Amsterdam) **303**, 2 (2003).

[14] C. Nayak, S. H. Simon, A. Stern, M. Freedman, and S. D. Sarma, Rev. Mod. Phys. **80**, 1083 (2008).

[15] G. Moore and N. Read, Nucl. Phys. **B360**, 362 (1991).

[16] M. Greiter, X.-G. Wen, and F. Wilczek, Phys. Rev. Lett. **66**, 3205 (1991).

[17] N. Read and D. Green, Phys. Rev. B **61**, 10267 (2000).

[18] R. H. Morf, Phys. Rev. Lett. **80**, 1505 (1998).

[19] E. H. Rezayi and F. D. M. Haldane, Phys. Rev. Lett. **84**, 4685 (2000).

[20] X. Wan, K. Yang, and E. H. Rezayi, Phys. Rev. Lett. **97**, 256804 (2006).

[21] Z.-X. Hu, E. H. Rezayi, X. Wan, and K. Yang, Phys. Rev. B **80**, 235330 (2009).

[22] G. Möller and S. H. Simon, Phys. Rev. B **77**, 075319 (2008).

[23] M. R. Peterson, T. Jolicoeur, and S. D. Sarma, Phys. Rev. Lett. **101**, 016807 (2008).

[24] H. Wang, D. N. Sheng, and F. D. M. Haldane, Phys. Rev. B **80**, 241311(R) (2009).

[25] M. Storni, R. H. Morf, and S. D. Sarma, Phys. Rev. Lett. **104**, 076803 (2010).

[26] A. E. Feiguin, E. Rezayi, C. Nayak, and S. D. Sarma, Phys. Rev. Lett. **100**, 166803 (2008).

[27] M. Storni and R. H. Morf, Phys. Rev. B **83**, 195306 (2011).

[28] K. Pakrouski, M. R. Peterson, T. Jolicoeur, V. W. Scarola, C. Nayak, and M. Troyer, Phys. Rev. X **5**, 021004 (2015).

[29] W. Zhu, Z. Liu, F. D. M. Haldane, and D. N. Sheng, Phys. Rev. B **94**, 245147 (2016).

[30] A. Wójs, C. Tőke, and J. K. Jain, Phys. Rev. Lett. **105**, 096802 (2010).

[31] M. Levin, B. I. Halperin, and B. Rosenow, Phys. Rev. Lett. **99**, 236806 (2007).

[32] S.-S. Lee, S. Ryu, C. Nayak, and M. P. A. Fisher, Phys. Rev. Lett. **99**, 236807 (2007).

[33] M. P. Zaletel, R. S. K. Mong, F. Pollmann, and E. H. Rezayi, Phys. Rev. B **91**, 045115 (2015).

[34] E. H. Rezayi, Phys. Rev. Lett. **119**, 026801 (2017).

[35] B. Yang, Phys. Rev. B **98**, 201101(R) (2018).

[36] B. Yang, N. Jiang, X. Wan, J. Wang, and Z.-X. Hu, Phys. Rev. B **99**, 161108(R) (2019).

[37] M. Banerjee, M. Heiblum, V. Umansky, D. E. Feldman, Y. Oreg, and A. Stern, Nature (London) **559**, 205 (2018).

[38] P. T. Zucker and D. E. Feldman, Phys. Rev. Lett. **117**, 096802 (2016).

[39] X. Chen, L. Fidkowski, and A. Vishwanath, Phys. Rev. B **89**, 165132 (2014).

[40] S. H. Simon, Phys. Rev. B **97**, 121406(R) (2018).

[41] D. E. Feldman, Phys. Rev. B **98**, 167401 (2018).

[42] S. H. Simon, Phys. Rev. B **98**, 167402 (2018).

[43] K. K. W. Ma and D. E. Feldman, Phys. Rev. B **99**, 085309 (2019).

[44] D. F. Mross, Y. Oreg, A. Stern, G. Margalit, and M. Heiblum, Phys. Rev. Lett. **121**, 026801 (2018).

[45] C. Wang, A. Vishwanath, and B. I. Halperin, Phys. Rev. B **98**, 045112 (2018).

[46] B. Lian and J. Wang, Phys. Rev. B **97**, 165124 (2018).

[47] X. Wan and K. Yang, Phys. Rev. B **93**, 201303(R) (2016).

[48] X.-G. Wen, *Quantum Field Theory of Many-Body Systems: From the Origin of Sound to an Origin of Light and Electrons* (Oxford, 2004).

[49] H. Li and F. D. M. Haldane, Phys. Rev. Lett. **101**, 010504 (2008).

[50] X.-L. Qi, H. Katsura, and A. W. W. Ludwig, Phys. Rev. Lett. **108**, 196402 (2012).

[51] E. Keski-Vakkuri and X.-G. Wen, Int. J. Mod. Phys. B **07**, 4227 (1993).

[52] S. D. Sarma, M. Freedman, and C. Nayak, Phys. Rev. Lett. **94**, 166802 (2005).

[53] A. Stern and B. I. Halperin, Phys. Rev. Lett. **96**, 016802 (2006).

[54] P. Bonderson, A. Kitaev, and K. Shtengel, Phys. Rev. Lett. **96**, 016803 (2006).

[55] P. Fendley, M. P. A. Fisher, and C. Nayak, Phys. Rev. Lett. **97**, 036801 (2006).

[56] M. Milovanovic and N. Read, Phys. Rev. B **53**, 13559 (1996).

[57] N. P. Sandler, C. C. Chamon, and E. Fradkin, Phys. Rev. B **57**, 12324 (1998).

[58] A. Kapustin and N. Saulina, Nucl. Phys. **B845**, 393 (2011).

[59] A. Kitaev and L. Kong, Commun. Math. Phys. **313**, 351 (2012).

[60] M. Barkeshli, C.-M. Jian, and X.-L. Qi, Phys. Rev. B **88**, 241103(R) (2013).

[61] M. Levin, Phys. Rev. X **3**, 021009 (2013).

[62] Y.-M. Lu and D.-H. Lee, Phys. Rev. B **89**, 205117 (2014).

[63] J. Cano, M. Cheng, M. Barkeshli, D. J. Clarke, and C. Nayak, Phys. Rev. B **92**, 195152 (2015).

[64] J. C. Wang and X.-G. Wen, Phys. Rev. B **91**, 125124 (2015).

[65] T. Lan, J. C. Wang, and X.-G. Wen, Phys. Rev. Lett. **114**, 076402 (2015).

[66] K. Yang, Phys. Rev. B **96**, 241305(R) (2017).

[67] L. H. Santos, J. Cano, M. Mulligan, and T. L. Hughes, Phys. Rev. B **98**, 075131 (2018).

[68] V. Crpel, N. Claussen, N. Regnault, and B. Estienne, Nat. Commun. **10**, 1860 (2019).

[69] V. Crpel, N. Claussen, B. Estienne, and N. Regnault, Nat. Commun. **10**, 1861 (2019).

[70] V. Crépel, B. Estienne, and N. Regnault, Phys. Rev. Lett. **123**, 126804 (2019).

[71] B. Jaworowski and A. E. B. Nielsen, Phys. Rev. B **101**, 245164 (2020).

[72] E. Grosfeld and K. Schoutens, Phys. Rev. Lett. **103**, 076803 (2009).

[73] F. A. Bais, J. K. Slingerland, and S. M. Haaker, Phys. Rev. Lett. **102**, 220403 (2009).

[74] M. Barkeshli, M. Mulligan, and M. P. A. Fisher, Phys. Rev. B **92**, 165125 (2015).

[75] C. de C. Chamon and X. G. Wen, Phys. Rev. B **49**, 8227 (1994).

[76] X. Wan, K. Yang, and E. H. Rezayi, Phys. Rev. Lett. **88**, 056802 (2002).

[77] X. Wan, E. H. Rezayi, and K. Yang, Phys. Rev. B **68**, 125307 (2003).

[78] T. Can, P. J. Forrester, G. Téllez, and P. Wiegmann, Phys. Rev. B **89**, 235137 (2014).

[79] See Supplemental Material at http://link.aps.org/supplemental/10.1103/PhysRevLett.125.146802 for more details of the calculation and results to support the discussion in the main text (Secs. A–E), which includes Refs. [30,33,44–47,51,80–85].

[80] M. P. Zaletel, R. S. K. Mong, and F. Pollmann, Phys. Rev. Lett. **110**, 236801 (2013).

[81] Y. J. Park and F. D. M. Haldane, Phys. Rev. B **90**, 045123 (2014).

[82] S. H. Simon, M. Ippoliti, M. P. Zaletel, and E. H. Rezayi, Phys. Rev. B **101**, 041302(R) (2020).

[83] D. T. Son, Phys. Rev. X **5**, 031027 (2015).

[84] W. Zhu, S. S. Gong, F. D. M. Haldane, and D. N. Sheng, Phys. Rev. Lett. **115**, 126805 (2015).

[85] S. D. Geraedts, M. P. Zaletel, R. S. K. Mong, M. A. Metlitski, A. Vishwanath, and O. I. Motrunich, Science **352**, 197 (2016).

[86] S. R. White, Phys. Rev. Lett. **69**, 2863 (1992).

[87] I. P. McCulloch, arXiv:0804.2509.

[88] X. G. Wen and A. Zee, Phys. Rev. Lett. **69**, 953 (1992).

[89] Y.-L. Wu, B. Estienne, N. Regnault, and B. A. Bernevig, Phys. Rev. Lett. **113**, 116801 (2014).

[90] E. J. Bergholtz and A. Karlhede, Phys. Rev. Lett. **94**, 026802 (2005).

[91] B. A. Bernevig and F. D. M. Haldane, Phys. Rev. Lett. **100**, 246802 (2008).

[92] J. E. Avron, R. Seiler, and P. G. Zograf, Phys. Rev. Lett. **75**, 697 (1995).

[93] F. Haldane, arXiv:0906.1854.

[94] F. D. M. Haldane, Phys. Rev. Lett. **107**, 116801 (2011).

[95] N. Read, Phys. Rev. B **79**, 045308 (2009).

[96] N. Read and E. H. Rezayi, Phys. Rev. B **84**, 085316 (2011).

[97] W. Zhu and D. N. Sheng, Phys. Rev. Lett. **123**, 056804 (2019).